

## Research Article

Yijie Shen\*, Eduardo Casas Martínez, and Carmelo Rosales-Guzmán\*

# Generation of tunable optical skyrmions on Skyrme-Poincaré sphere

<https://doi.org/10.1515/sample-YYYY-XXXX>

Received Month DD, YYYY; revised Month DD, YYYY; accepted Month DD, YYYY

**Abstract:** In recent time, the optical-analogous skyrmions, topological quasiparticles with sophisticated vectorial structures, have received an increasing amount of interest. Here we propose theoretically and experimentally a generalized family of these, the tunable optical skyrmion, unveiling a new mechanism to transform between various skyrmionic topologies, including Néel-, Bloch-, and anti-skyrmion types, via simple parametric tuning. In addition, Poincaré-like geometric representation is proposed to visualize the topological evolution of tunable skyrmions, which we termed Skyrme-Poincaré sphere, akin to the spin-orbit representation of complex vector modes. To generate experimentally the tunable optical skyrmions we implemented a digital hologram system based on a spatial light modulator, showing great agreement with our theoretical prediction.

**Keywords:** Optical skyrmions, topology, structured light, vector beams, Poincaré sphere.

## 1 Introduction

Skyrmions are topologically protected quasiparticle in high-energy physics and condensed matter with salient vectorial textures [1, 2]. This concept was recently identified by the optics and photonics community as a cutting-edge topic. Recently, skyrmions were constructed in optical field as state-of-the-art optical structures and termed optical

skyrmions [3]. These were first generated in the electric field of evanescent wave [3] followed by diverse forms constructed from different kinds of optical fields, such as, spin field of confined free-space waves [4, 5], Stokes vectors of paraxial vector beams [6, 7], magnetic vectors in propagating light pulses [8], and pseudospins in photonic crystals [9]. The creation of optical skyrmions has promising advanced applications in fields such as nanoscale metrology [10], deep-subwavelength microscopy [4], ultrafast vector imaging [11], and topological Hall devices [9], broadening the frontier of modern fundamental and applied physics.

The advancement skyrmions provide is mainly on their versatile topological textures, providing new degrees of freedom to shape vectorial fields and encode information. The skyrmionic configuration can be mapped into real-space magnetic materials and classified into diverse topologies [12, 13], including Néel-type [14], Bloch-type [15], and anti-skyrmion [16]. However, the control of diverse topologies of optical skyrmions is an emerging topic still its infancy. As the first scheme of optical skyrmions, the evanescent electric fields on a plasmonic surface can only form Néel-type skyrmions [3, 11]. One year ago, a study of plasmonic skyrmion controlled between Néel- and Bloch-types was reported [17], but, soon after, such Bloch-type skyrmion was disproved [18, 19]. The loophole-free observation of Bloch-type optical skyrmion was reported very recently in optical chiral multilayers [20]. For the optical skyrmions in free space, Bloch-type skyrmion was proved in spin field of a tightly focused vortex beam [4]. And soon after, both Néel- and Bloch-type skyrmions were theoretically presented in Stokes vectors of paraxial vector beams [6] and electric-spin fields in tightly focused vector beams [5], however, no experimental results have been reported for free-space skyrmions. Finally, the optical anti-skyrmion also has never been proposed yet.

In this paper, a closed-form expression is proposed to characterize a general class of optical skyrmions, where skyrmions with different textures (Néel-, Bloch-, and anti-skyrmion types) can be topologically transformed among each others via simple parametric tuning. Moreover, a novel geometrical model, Skyrme-Poincaré sphere, is proposed to universally map the topological transformation

**\*Corresponding author: Yijie Shen**, Optoelectronics Research Centre, University of Southampton, Southampton SO17 1BJ, United Kingdom, e-mail: y.shen@soton.ac.uk

**Eduardo Casas Martínez**, Instituto Nacional de Astrofísica, Óptica y Electrónica, Departamento de Óptica, Puebla, México

**\*Corresponding author: Carmelo Rosales-Guzmán**, Centro de Investigaciones en Óptica, A.C., Loma del Bosque 115, Colonia Lomas del campestre, 37150 León, Gto., Mexico, e-mail: carmelorosalesg@cio.mx; and Wang Da-Heng Collaborative Innovation Center, Heilongjiang Provincial Key Laboratory of Quantum Manipulation and Control, Harbin University of Science and Technology, Harbin 150080, China, e-mail: carmelorosalesg@hrbust.edu.cn

of tunable optical skyrmions, akin to the prior modal Poincaré sphere representing spin-orbital conversation. Importantly, we experimentally generate the tunable optical skyrmions with all the topological types in structured vector beams controlled by a digital hologram system, showing great agreement with our theoretical prediction.

## 2 Theory

### 2.1 Topologies of skyrmions

Topological properties of a skyrmionic configuration can be characterized by the skyrmion number defined by [13]:

$$s = \frac{1}{4\pi} \iint_{\sigma} \mathbf{n} \cdot \left( \frac{\partial \mathbf{n}}{\partial x} \times \frac{\partial \mathbf{n}}{\partial y} \right) dx dy \quad (1)$$

where  $\mathbf{n}(x, y)$  represents the vector field to construct a skyrmion and  $\sigma$  the region to confine the skyrmion, which can be infinity (for an isolated skyrmion) also can be a cell of a periodic distribution (for skyrmion lattices). The skyrmion number is an integer counting how many times the vector  $\mathbf{n}(x, y) = \mathbf{n}(r \cos \theta, r \sin \theta)$  wraps around the unit sphere, as the mapping shown in Fig. 1(a). For mapping to the unit sphere, the vector can be given by  $\mathbf{n} = (\cos \alpha(\theta) \sin \beta(r), \sin \alpha(\theta) \sin \beta(r), \cos \beta(r))$ . Also, the skyrmion number can be separated into two integers:

$$s = \frac{1}{4\pi} \int_0^{r_\sigma} dr \int_0^{2\pi} d\theta \frac{d\beta(r)}{dr} \frac{d\alpha(\theta)}{d\theta} \sin \beta(r) \\ = \frac{1}{4\pi} [\cos \beta(r)]_{r=0}^{r=r_\sigma} [\alpha(\theta)]_{\theta=0}^{\theta=2\pi} = p \cdot m \quad (2)$$

the polarity,  $p = \frac{1}{2} [\cos \beta(r)]_{r=0}^{r=r_\sigma}$ , indicates the direction of the vector down (up) at center  $r = 0$  and up (down) at boundary  $r \rightarrow r_\sigma$  for  $p = 1$  ( $p = -1$ ), and the vorticity,  $m = \frac{1}{2\pi} [\alpha(\theta)]_{\theta=0}^{\theta=2\pi}$ , controls the distribution of the transverse field components [21]. In the case of a helical distribution, an initial phase  $\gamma$  should be added,  $\alpha(\theta) = m\theta + \gamma$ . If we consider the transverse vector components at a given radius (or a given latitude angle  $\beta$  in the unit-sphere representation), the  $\gamma$  reveals the inclined angle of initial vector in the circular array, see Fig. 1(b). For the  $m = 1$  skyrmion, the cases of  $\gamma = 0$  and  $\gamma = \pi$  are classified as Néel-type, and the cases of  $\gamma = \pm\pi/2$  are Bloch-type. The case of  $m = -1$  is anti-skyrmion.

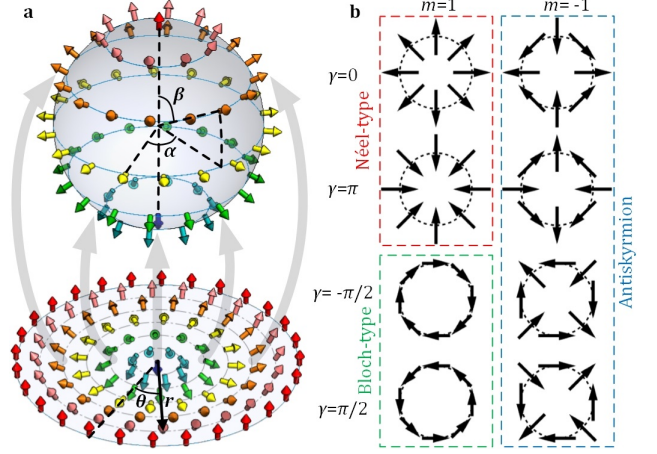


**Fig. 1:** (a) The mapping from a normal skyrmion configuration, constructed by the colored arrows, to the unit sphere representation. (b) Some basic cases of the transversely projected vector ( $E_x$  and  $E_y$  components) distribution at a given radius of the skyrmions with various values of  $m$  and  $\gamma$ .

### 2.2 Tunable optical skyrmions

In order to derive a closed-form expression that allows to tune between optical skyrmions with diverse topological textures via simple parameters, we start by a classic model of optical skyrmion, which was also the first model of optical skyrmion. Namely, the skyrmionic vector field,  $\mathbf{n} = (n_x, n_y, n_z)$ , is constructed by the electric field vectors,  $(E_x, E_y, E_z)^T / |\mathbf{E}|$ , in a confined surface plasmon polaritons (SPP) wave [3]:

$$\mathbf{n} = E_0 e^{-|k_z|z} \sum_{n=1}^N \begin{pmatrix} -\frac{|k_z|z \cos \theta_n}{k_{\parallel}} \sin(k_{\parallel} \mathbf{r}_{\parallel} \cdot \boldsymbol{\theta}_n) \\ -\frac{|k_z|z \sin \theta_n}{k_{\parallel}} \sin(k_{\parallel} \mathbf{r}_{\parallel} \cdot \boldsymbol{\theta}_n) \\ \cos(k_{\parallel} \mathbf{r}_{\parallel} \cdot \boldsymbol{\theta}_n) \end{pmatrix} \quad (3)$$

where  $E_0$  is a normalized amplitude,  $k_{\parallel}$  and  $k_z$  are transverse (in-plane) and axial wavenumbers,  $\mathbf{r}_{\parallel} = (x, y)$  and  $\boldsymbol{\theta}_n = (\cos \theta_n, \sin \theta_n)$ . The physical meaning of Eq. (3) is the superposition of  $N$  standing-wave SPPs along directions with equally distributed in-plane angles  $\theta_n$  ( $n = 1, 2, \dots, N$ ). For common circular-shape skyrmions,  $N$  should large enough, ideally  $N \rightarrow \infty$ . For the case of skyrmion lattice,  $N$  should be a integer related to the boundary geometry, e.g.  $N = 3$  is set for simulating hexagonal skyrmion-lattice field with  $\theta_n = [-\pi/3, 0, \pi/3]$  [3]. Figure 2(a) shows a simulated result of skyrmionic vector distribution using Eq. (3). However, Eq. (3) can only represent Néel-type skyrmion (lattice). Here we propose a

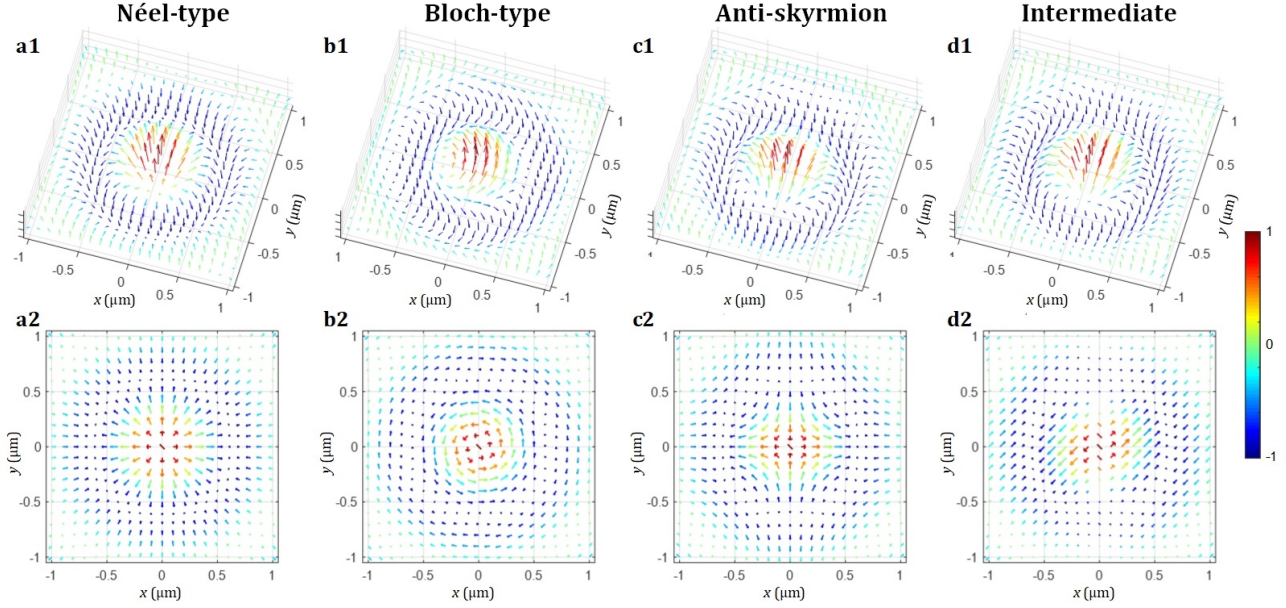


**Fig. 2:** (a-d) The simulated results (a1-d1) The 3D vector distributions,  $(n_x, n_y, n_z)$  and (a2-d2) the transverse component vectors,  $(n_x, n_y)$ , for tunable optical skyrmions with diverse topological textures of Néel-type (a,  $\phi_1 = \phi_2 = 0$ ), Bloch-type (b,  $\phi_1 = \phi_2 = \pi/2$ ), anti-skyrmion (c,  $\phi_1 = 0, \phi_2 = \pi$ ), and an intermediate state (d,  $\phi_1 = 0, \phi_2 = \pi/2$ ), respectively, and other Parameters used in simulation:  $k_z = 2\pi \text{ nm}^{-1}$ ,  $k_{\parallel} = 2k_z$ ,  $N = 3$ ,  $\phi_1$  and  $\phi_2$ .

mathematically generalized form that breaks this limit:

$$\mathbf{n} = E_0 e^{-|k_z|z} \sum_{n=1}^N \begin{pmatrix} -\frac{|k_z| \cos(\theta_n + \phi_1)}{k_{\parallel}} \sin(k_{\parallel} \mathbf{r}_{\parallel} \cdot \boldsymbol{\theta}_n) \\ -\frac{|k_z| \sin(\theta_n + \phi_2)}{k_{\parallel}} \sin(k_{\parallel} \mathbf{r}_{\parallel} \cdot \boldsymbol{\theta}_n) \\ \cos(k_{\parallel} \mathbf{r}_{\parallel} \cdot \boldsymbol{\theta}_n) \end{pmatrix} \quad (4)$$

Compared with Eq. (3), Eq. (4) has two additional parameters,  $\phi_1$  and  $\phi_2$ , the control of which can drive the skyrmionic vector field to cover all the three types of topologies (Néel-, Bloch- and anti-skyrmion). For  $\phi_1 = \phi_2 = \phi \in [0, 2\pi]$ , Eq. (4) represents tunable skyrmion between Néel- ( $\phi = 0, \pi$ ) and Bloch-types ( $\phi = \pi/2, 3\pi/2$ ), see **Video 1** for the evolution movie and a result of the Bloch-type skyrmion, which is shown in Figs. 2(b). For  $\phi_1 = 0$  and  $\phi_2 = \phi \in [0, 2\pi]$ , Eq. (4) represents tunable skyrmion between Néel-type ( $\phi = 0$ ) and anti-skyrmion ( $\phi = \pi$ ), see **Video 2** for the movie, a result of an anti-skyrmion in Figs. 2(c) and an interposed state in such transformation is shown in Figs. 2(d). When  $\phi_1 = \pi/2$  and  $\phi_2 = \phi \in [0, 2\pi]$ , Eq. (4) represents tunable skyrmion between Bloch-type ( $\phi = \pi/2$ ) and anti-skyrmion ( $\phi = 3\pi/2$ ), see **Video 3** for the movie.

The mathematical representation of Eq. (4) is correct for tunable optical skyrmion, but its experimental realization is still cumbersome. Attempting to use SPP to generate tunable skyrmions, as described by Eq. (4), the two parameters  $\phi_1$  and  $\phi_2$  would induce extreme conditions that are hard to fulfill, as a stable SPP field

requires rigorous conditions than a free-space light field. Importantly, recent advancements had made possible to successfully realize optical skyrmions with different optical vector fields in both matter and free space [4–6, 9]. These advancements allows to propose a practical scheme for the generation of tunable optical skyrmions in free space, via the Stokes vectors of structured vector beams. The Stokes vector  $\mathbf{s} = (s_1, s_2, s_3)$  can represent an arbitrary state of polarization, as points on the surface of unit-radius sphere known as the Poincaré sphere [22]. In spherical coordinates, the optical field  $\boldsymbol{\psi} = \cos(\theta/2)e^{-i\varphi/2}\mathbf{R} + \sin(\theta/2)e^{i\varphi/2}\mathbf{L}$ , where  $\mathbf{R}$  and  $\mathbf{L}$  represent right- and left-handed circularly polarized (RCP and LCP) eigenstates, respectively, is represented as  $\mathbf{s} = (\cos\varphi \sin\theta, \sin\varphi \sin\theta, \cos\theta)$ . In order to construct skyrmions by Stokes vector, we need to first construct a vector beam with customized spatial modes of the form,

$$\boldsymbol{\psi}(x, y) = \psi_1(x, y)\mathbf{R} + \psi_2(x, y)\mathbf{L}. \quad (5)$$

The spatial modes  $\psi_1$  and  $\psi_2$  should have the same form of the tunable skyrmion, given by Eq. (4), that is,

$$\psi_1(x, y) = \cos[\theta(x, y)/2]e^{-i\varphi(x, y)/2} \quad (6)$$

$$\psi_2(x, y) = \sin[\theta(x, y)/2]e^{i\varphi(x, y)/2}, \quad (7)$$

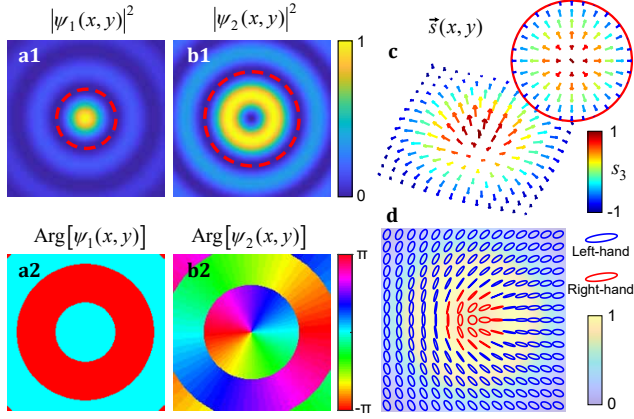


**Fig. 3:** (a,b) Intensity (a1,b1) and phase (a2,b2) distributions of  $\psi_1(x, y)$  (a) and  $\psi_2(x, y)$  (b) for the case of  $\phi_1 = \phi_2 = 0$ , the red-dash lines mark the effective regions to induce optical skyrmion. (c,d) The skyrmion in Stokes vector field with transverse component inset (c) and the intensity and polarization distributions (d) of the corresponding vector beam.

with

$$\theta(x, y) = \cos^{-1}[n_z(x, y)] \quad (8)$$

$$\varphi(x, y) = \sin^{-1} \left[ \frac{n_y(x, y)}{\sin \theta(x, y)} \right] = \cos^{-1} \left[ \frac{n_x(x, y)}{\sin \theta(x, y)} \right] \quad (9)$$

where,  $(n_x, n_y, n_z)$  is exactly based on theoretical tunable skyrmion of Eq. (4). We can now tailor vector beams to realize tunable skyrmions via their Stokes vector fields. As a way of example, a numerical simulation of the Néel-type skyrmionic vector beam, for which  $\phi_1 = \phi_2 = 0$ , is shown in Fig. 3. The spatial modes  $\psi_1(x, y)$  and  $\psi_2(x, y)$  are shown in Figs. 3(a,b), which share the same form of zero- and first-order Bessel modes, respectively. The simulation results also show that the effective regions to induce an skyrmionic structure are the central lobes of the zero- and first-order Bessel modes, as marked by red-dashed lines in Figs. 3(a,b). Importantly, the contribution of the outside rings, far away the skyrmion center, is almost negligible, which means, we can replace the zero- and first-order Bessel modes by the fundamental Gaussian and first-order Laguerre-Gaussian (LG) modes. The Stokes vector field of the corresponding vector beam given by Eq. (5) shows a perfect Néel-type skyrmion, as evinced in Figs. 3(c,d).

## 2.3 Skyrme-Poincaré sphere

In this section we present a graphical model, which we termed *Skyrme-Poincaré sphere*, to depict the general topological transformation of tunable skyrmion onto a Poincaré-like sphere. Without loss of generality, setting

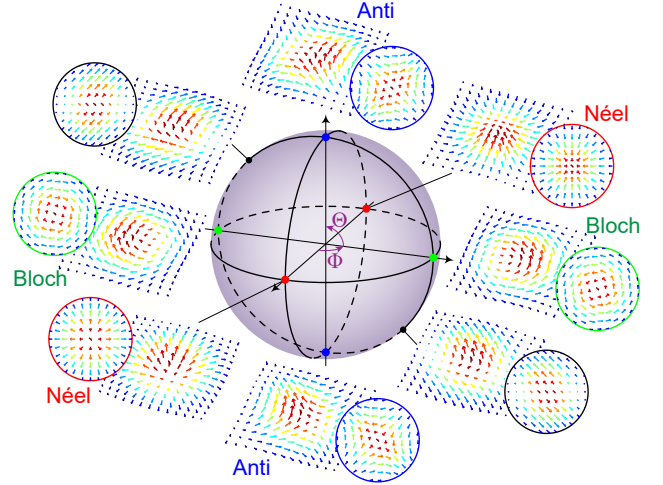


**Fig. 4:** The Skyrme-Poincaré sphere to represent universal topological evolution of tunable optical skyrmion, with special topology as a point on it: Red points, Néel-type; green points, Bloch-type; Blue points (the poles), anti-skyrmion.

$\phi_1 = \Phi \in [0, 2\pi]$  and  $(\phi_2 - \phi_1)/2 = \Theta \in [-\pi/2, \pi/2]$ , we can regard  $\Phi$  and  $\Psi$  as angles of longitude and latitude, respectively, to map the corresponding topological skyrmion to a corresponding point on the Skyrme-Poincaré sphere, as shown in Fig. 4. For  $\Theta = 0$ , the skyrmion transforms between Néel ( $\Phi = 0, \pi$ ) and Bloch ( $\Phi = \pm\pi/2$ ), which are represented on the equator. The anti-skyrmions are located at the poles, for  $\Theta = 0$  and  $\Theta = \pm\pi/2$ , which are independent of  $\Phi$ . This topology is extremely similar to the classic Poincaré sphere or modal Poincaré sphere that maps the evolution of spin/polarization or orbital angular momentum (OAM) of light [23–25], where the equator represents the non-spin or non-OAM modes, while the route from equator to the poles corresponds to the introducing of spin or OAM charge. Similarly in Skyrme-Poincaré sphere, the equatorial transformation is skyrmion-number-conserved, e.g., for the normal polarity  $p = 1$ , the skyrmion number is always  $s = 1$  for the tunable skyrmion between Néel and Bloch. While, the area from equator to the poles reveals the transformation to anti-skyrmion ( $s = -1$ ) introducing a fractional skyrmion-number evolution, akin to the fractional OAM evolution from equation to poles on a Poincaré sphere.

The Skyrme-Poincaré sphere has more sophisticated relation to OAM Poincaré sphere under the skyrmionic vector beam representation. Based on the methods introduced in last section, we can derive the parametric form

of corresponding vector beam dependent on  $\Phi$  and  $\Theta$ :

$$\Psi = \Psi_0 \mathbf{R} + \underbrace{\left[ \cos(\Theta/2) e^{-i\Phi/2} \Psi_{-1} + \sin(\Theta/2) e^{i\Phi/2} \Psi_1 \right]}_{\text{OAM Poincaré sphere}} \mathbf{L} \quad (10)$$

where  $\Psi_0$  is zero-order Bessel (or fundamental Gaussian) mode and  $\Psi_{\pm 1}$  are  $\pm 1$ th-order Bessel modes (or LG modes) carrying opposite OAM with  $\pm 1$  topological charges. And the spatial mode of LCP component is exactly the form of conventional OAM Poincaré sphere driven by the longitude and latitude angles  $\Phi$  and  $\Theta$ , revealing the OAM conversion between  $\pm 1$  topological charges. Therefore the Skyrme-Poincaré sphere representing skyrmionic topological transformation can be bidirectionally mapped to conventional OAM Poincaré sphere representing OAM transformation. As such, many Poincaré-related applications, such as spin-orbit conversion, geometric phase transition, encoding and communication [22, 24, 26], are expected to transfer to optical skyrmion.

### 3 Experiment

In order to realize experimentally the tunable optical skyrmions, we implemented a highly stable optical setup capable to generate arbitrary optical beams with almost any state of polarisation and spatial profile [27], which is schematically shown in Fig. 5. Such optical setup comprises the use of a Spatial Light Modulator (SLM) for arbitrary control of the spatial distribution of the optical field [28]. The setup starts with a horizontally polarised HeNe (632.8 nm) laser beam, collimated and expanded to fully cover the liquid crystal screen of the SLM. The screen of the SLM is digitally split into two independent screens, each of which is addressed with an independent digital hologram that generates, in the first diffraction order, two independent optical fields. Each digital hologram is superimposed with a linear grating to separate the different diffraction orders. Afterwards, the first diffraction order is spatially filtered using a telescope formed by two lenses and a spatial filter. Afterwards, the two optical fields are redirected to a common-path triangular Sagnac interferometer comprising a Polarising Beam Splitter (PBS) and two mirrors. Prior to entering the interferometer, both beams are rotated to a diagonal polarisation state. In this way, when both beams enter the interferometer, after traversing the PBS, each of them is separated into two new beams with orthogonal linear polarisation states, horizontal and vertical, traveling along opposite optical paths.

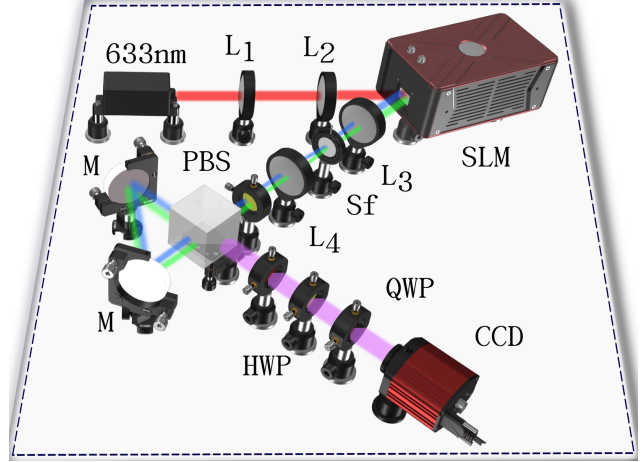


**Fig. 5:** Schematic representation of the optical setup implemented to generate tunable optical skyrmions.  $L_1 - L_4$ : lenses, PBS: Polarizing Beam Splitter, SLM: Spatial Light Modulator, HWP: Half-Wave plate, QWP: Quarter-Wave Plate, M: Mirror, SF: Spatial Filter, CCD: Charge Coupled Device Camera

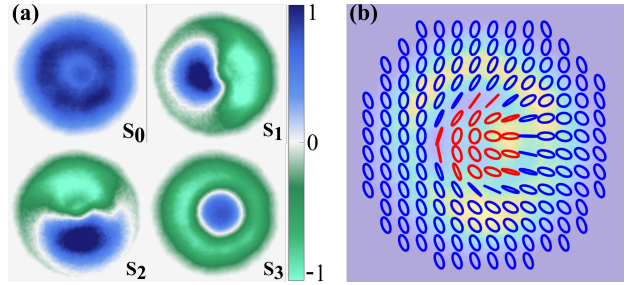


**Fig. 6:** Experimentally reconstructed (a) Stokes parameters and (b) intensity distribution of the vector field overlapped with its corresponding polarisation distribution.

After a round trip, all four beams exit the interferometer from the opposite side of the PBS, two with horizontal polarization and two with vertical. Finally, the horizontal polarisation component of one of the beams is aligned co-axially with the vertical polarisation component of the other beam. To ensure a perfect coaxial superposition, a fine tuning is performed digitally by adjusting the period of the linear gratings encoded on each digital hologram.

The experimental reconstruction of the optical skyrmions was achieved through Stokes polarimetry, more specifically, through the reconstruction of the Stokes parameters  $S_0$ ,  $S_1$ ,  $S_2$  and  $S_3$ , which were computed from a set of intensity measurements. To this end, a second stage was built at the output port of the interferometer, where a series of phase retarders and a Charge-Coupled Device (CCD) camera allowed to measure the required intensities, from which the Stokes parameters were reconstructed.

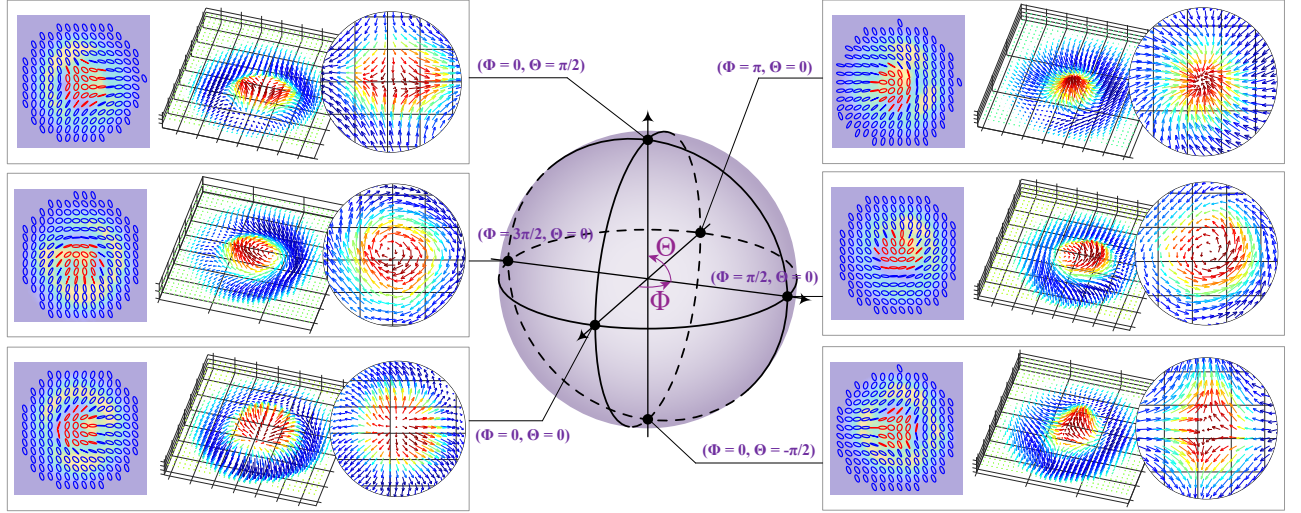


**Fig. 7:** Experimentally results of tunable Stokes skyrmions with controlled topological textures corresponding to selective points on Skyrme-Poincaré sphere (see gray boxes), each box include the measured intensity and polarization distribution of the skyrmionic beam, the vector distribution of the Stokes skyrmions, and the zoom-in planform of the vector field for clearly distinguishing the topological texture.

using the relations,

$$\begin{aligned} S_0 &= I_H + I_V, & S_1 &= 2I_H - S_0, \\ S_2 &= 2I_D - S_0, & S_3 &= 2I_R - S_0, \end{aligned} \quad (11)$$

where,  $I_H$ ,  $I_V$ ,  $I_D$  and  $I_R$  represent the intensity of the horizontal, vertical, diagonal and right-handed polarisation components, respectively. To experimentally measure  $I_H$ ,  $I_V$  and  $I_D$  we passed the optical field through a linear polariser set at  $0^\circ$ ,  $45^\circ$  and  $95^\circ$ , respectively, while the intensity of the  $I_R$  polarisation component was acquired by passing it simultaneously through a QWP at  $45^\circ$  and a linear polariser at  $90^\circ$  (see [29] for further details). Figure 6(a) show an example of the experimental Stokes parameters along with the intensity profile overlapped with its corresponding polarization distribution, Fig. 6(a), for the specific case  $\phi_1 = \phi_2 = 0$ .

With our digital hologram system, we realized a controlled generation of Stokes skyrmions with arbitrary topological textures on the Skyrme-Poincaré sphere. Figure 7 shows our experimentally generated LG-based results of tunable Stokes skyrmions on typical points of Skyrme-Poincaré sphere, including the measured intensity and polarization distributions, Stokes vector fields, and the zoom-in planforms of the vector field for clearly distinguishing the topological textures. See more experiential results in Supplementary materials (Video 4 and Video 5 for the LG mode and Bessel mode based results).

## 4 Discussion

Although the generalized tunable optical skyrmion model is inspired from the case of SPP electric field, and realized by Stokes vector field, it is not limited in these cases and can be freely extendable. Because the new concept of tunable skyrmion has a universal mathematical parametrization for generalized topology, the vector can refer to other kinds of optical field of structured light for the further exploration. For example, we can also use spin vectors in a tightly focused beam [4, 5], electric or magnetic vectors in a propagating structured pulse [8], and pseudospins in nonlinear media [9]. It is also a exciting direction to create more quasiparticle with complex topological states beyond skyrmions, such as skyrmion bags [30] and skyrmion tubes [31], meron and bimeron [32–34], into structured light. Even though in this work, we used an SLM to generate skyrmionic beams, Digital Mirror Devices represent an alternative means to generated them, which present several advantages over SLMs, such as, their high refresh rates, polarisation independence and low cost[29].

Conclusively, we proposed an extended family of tunable optical skyrmion, enabling flexible transformation among various kinds of skyrmionic topological textures. A graphical model, Skyrme-Poincaré sphere, is proposed to universally represent the topological evolution of tunable optical skyrmion. We experimentally generated such tunable optical skyrmions in Stokes vector fields of customized

vector beams from a well-designed digital hologram system. This is the first-known experimental generation of topology-tunable optical skyrmions in free space, also the first realization of optical anti-skyrmions. Our methods provide a new platform for optical information storage, communication, and cryptography using skyrmionic topological states of light.

**Funding:** National Natural Science Foundation of China (61975047).

## References

- [1] Börge Göbel, Ingrid Mertig, and Oleg A Tretiakov. Beyond skyrmions: Review and perspectives of alternative magnetic quasiparticles. *Physics Reports*, 895:1–28, 2021.
- [2] Albert Fert, Nicolas Reyren, and Vincent Cros. Magnetic skyrmions: advances in physics and potential applications. *Nature Reviews Materials*, 2(7):1–15, 2017.
- [3] S Tsesses, E Ostrovsky, K Cohen, B Gjonaj, NH Lindner, and G Bartal. Optical skyrmion lattice in evanescent electromagnetic fields. *Science*, 361(6406):993–996, 2018.
- [4] Luping Du, Aiping Yang, Anatoly V Zayats, and Xiaocong Yuan. Deep-subwavelength features of photonic skyrmions in a confined electromagnetic field with orbital angular momentum. *Nature Physics*, 15(7):650–654, 2019.
- [5] Rodrigo Gutiérrez-Cuevas and Emilio Pisanty. Optical polarization skyrmionic fields in free space. *Journal of Optics*, 23(2):024004, 2021.
- [6] Sijia Gao, Fiona C Speirits, Francesco Castellucci, Sonja Franke-Arnold, Stephen M Barnett, and Jörg B Götze. Paraxial skyrmionic beams. *Physical Review A*, 102(5):053513, 2020.
- [7] Wenbo Lin, Yasutomo Ota, Yasuhiko Arakawa, and Satoshi Iwamoto. Microcavity-based generation of full poincaré beams with arbitrary skyrmion numbers. *Physical Review Research*, 3(2):023055, 2021.
- [8] Yijie Shen, Yaonan Hou, Nikitas Papasimakis, and Nikolay I Zheludev. Supertoroidal light pulses: Propagating electromagnetic skyrmions in free space. *arXiv preprint arXiv:2103.08431*, 2021.
- [9] Aviv Karnieli, Shai Tsesses, Guy Bartal, and Ady Arie. Emulating spin transport with nonlinear optics, from high-order skyrmions to the topological hall effect. *Nature Communications*, 12(1):1–9, 2021.
- [10] Yanan Dai, Zhikang Zhou, Atreyee Ghosh, Roger SK Mong, Atsushi Kubo, Chen-Bin Huang, and Hrvoje Petek. Plasmonic topological quasiparticle on the nanometre and femtosecond scales. *Nature*, 588(7839):616–619, 2020.
- [11] Timothy J Davis, David Janoschka, Pascal Dreher, Bettina Frank, Frank-J Meyer zu Heringdorf, and Harald Giessen. Ultrafast vector imaging of plasmonic skyrmion dynamics with deep subwavelength resolution. *Science*, 368(6489), 2020.
- [12] XZ Yu, Yoshinori Onose, Naoya Kanazawa, JH Park, JH Han, Yoshio Matsui, Naoto Nagaosa, and Yoshinori Tokura. Real-space observation of a two-dimensional skyrmion crystal. *Nature*, 465(7300):901–904, 2010.
- [13] Naoto Nagaosa and Yoshinori Tokura. Topological properties and dynamics of magnetic skyrmions. *Nature Nanotechnology*, 8(12):899–911, 2013.
- [14] István Kézsmárki, Sándor Bordács, Peter Milde, E Neuber, LM Eng, JS White, Henrik M Rønnow, CD Dewhurst, M Mochizuki, K Yanai, et al. Néel-type skyrmion lattice with confined orientation in the polar magnetic semiconductor  $\text{GaV}_4\text{S}_8$ . *Nature Materials*, 14(11):1116–1122, 2015.
- [15] Dustin A Gilbert, Brian B Maranville, Andrew L Balk, Brian J Kirby, Peter Fischer, Daniel T Pierce, John Unguris, Julie A Borchers, and Kai Liu. Realization of ground-state artificial skyrmion lattices at room temperature. *Nature Communications*, 6(1):1–7, 2015.
- [16] Ajaya K Nayak, Vivek Kumar, Tianping Ma, Peter Werner, Eckhard Pippel, Roshnee Sahoo, Franoise Damay, Ulrich K Röbler, Claudia Felser, and Stuart SP Parkin. Magnetic antiskyrmions above room temperature in tetragonal heusler materials. *Nature*, 548(7669):561–566, 2017.
- [17] Chunyan Bai, Jian Chen, Yuxing Zhang, Dawei Zhang, and Qiwen Zhan. Dynamic tailoring of an optical skyrmion lattice in surface plasmon polaritons. *Optics Express*, 28(7):10320–10328, 2020.
- [18] Tim Meiler, Bettina Frank, and Harald Giessen. Dynamic tailoring of an optical skyrmion lattice in surface plasmon polaritons: comment. *Optics Express*, 28(22):33614–33615, 2020.
- [19] Chunyan Bai, Jian Chen, Dawei Zhang, and Qiwen Zhan. Dynamic tailoring of an optical skyrmion lattice in surface plasmon polaritons: reply. *Optics Express*, 28(22):33616–33618, 2020.
- [20] Qiang Zhang, Zhenwei Xie, Luping Du, Peng Shi, and Xiaocong Yuan. Bloch-type photonic skyrmions in optical chiral multilayers. *Physical Review Research*, 3(2):023109, 2021.
- [21] XS Wang, HY Yuan, and XR Wang. A theory on skyrmion size. *Communications Physics*, 1(1):1–7, 2018.
- [22] Carmelo Rosales-Guzmán, Bienvenu Ndagano, and Andrew Forbes. A review of complex vector light fields and their applications. *Journal of Optics*, 20(12):123001, 2018.
- [23] Miles J Padgett and Johannes Courtial. Poincaré-sphere equivalent for light beams containing orbital angular momentum. *Optics letters*, 24(7):430–432, 1999.
- [24] Mark R Dennis and Miguel A Alonso. Swings and roundabouts: optical poincaré spheres for polarization and gaussian beams. *Philosophical Transactions of the Royal Society A: Mathematical, Physical and Engineering Sciences*, 375(2087):20150441, 2017.
- [25] Yijie Shen, Zhaoyang Wang, Xing Fu, Darryl Naidoo, and Andrew Forbes. Su (2) poincaré sphere: A generalized representation for multidimensional structured light. *Physical Review A*, 102(3):031501, 2020.
- [26] Yijie Shen, Xuejiao Wang, Zhenwei Xie, Changjun Min, Xing Fu, Qiang Liu, Mali Gong, and Xiaocong Yuan. Optical vortices 30 years on: Oam manipulation from topological charge to multiple singularities. *Light: Science & Applications*, 8(90):1–29, 2019.
- [27] Benjamin Perez-Garcia, Carlos López-Mariscal, Raul I. Hernandez-Aranda, and Julio C. Gutiérrez-Vega. On-demand tailored vector beams. *Appl. Opt.*, 56(24):

- 6967–6972, Aug 2017. 10.1364/AO.56.006967. URL <http://ao.osa.org/abstract.cfm?URI=ao-56-24-6967>.
- [28] Carmelo Rosales-Guzmán and Andrew Forbes. *How to shape light with spatial light modulators*. SPIE Press, 2017. ISBN 9781510613027. URL <https://spie.org/publications/book/2281296?print=2{&}SSO=1>.
- [29] Carmelo Rosales-Guzmán, Xiao-Bo Hu, Adam Selyem, Pedro Moreno-Acosta, Sonja Franke-Arnold, Ruben Ramos-Garcia, and Andrew Forbes. Polarisation-insensitive generation of complex vector modes from a digital micromirror device. *Scientific Reports*, 10(1):10434, 2020. 10.1038/s41598-020-66799-9.
- [30] David Foster, Charles Kind, Paul J Ackerman, Jung-Shen B Tai, Mark R Dennis, and Ivan I Smalyukh. Two-dimensional skyrmion bags in liquid crystals and ferromagnets. *Nature Physics*, 15(7):655–659, 2019.
- [31] Hiroshi Kuratsuji and Satoshi Tsuchida. Evolution of the stokes parameters, polarization singularities, and optical skyrmion. *Physical Review A*, 103(2):023514, 2021.
- [32] Yijie Shen. Topological bimeronic beams. *Optics Letters*, 4:2, 2021.
- [33] Mateusz Król, Helgi Sigurdsson, Katarzyna Rechcińska, Przemysław Oliwa, Krzysztof Tyszka, Witold Bardyszewski, Andrzej Opala, Michał Matuszewski, Przemysław Morawiak, Rafał Mazur, et al. Observation of second-order meron polarization textures in optical microcavities. *Optica*, 8(2): 255–261, 2021.
- [34] Cheng Guo, Meng Xiao, Yu Guo, Luqi Yuan, and Shanhui Fan. Meron spin textures in momentum space. *Physical review letters*, 124(10):106103, 2020.